Hindawi
Advances in Meteorology
Volume 2019, Article ID 6292930, 11 pages
https://doi.org/10.1155/2019/6292930

Research Article

Differences in Cloud Vertical Structures between the Tibetan Plateau and Eastern China Plains during Rainy Season as Measured by CloudSat/CALIPSO

Mingjian Yi

Anhui Academy of Environmental Sciences Research, Hefei, Anhui, China

Correspondence should be addressed to Mingjian Yi; mjyi@ustc.edu.cn

Received 30 May 2019; Accepted 2 September 2019; Published 25 September 2019

Academic Editor: Anthony R. Lupo

Cloud vertical structures over the Tibetan Plateau (TP) and Eastern China Plains (ECP) were analyzed by using data in rainy seasons from 2006 to 2009, in order to clarify the cloud development over adjacent regions but with distinct topographies. Results indicate that the largest occurrences of cloud top height over the TP are at 7-8 km above mean sea level, which is about 4 km lower than that over the ECP. Mixed-phase clouds dominated more than 30% over the TP, while it is lower than 10% over the ECP. The infrequent mixed-phase clouds over the ECP are attributed to the unique dynamic and moisture situations over the downstream areas of the TP. Ice clouds have similar occurrences over the two regions. The prominent distinctions are manifested by the probability density of cloud thickness. The probability density of cloud thickness around 4–8 km is about 2% higher over the TP than the ECP. However, there is almost no ice cloud thicker than 10 km over the TP, while it is about 1% over the ECP. Compared with those over the ECP, every cloud layer within multilayered clouds is generally higher and thinner over the TP, which is closely related to the elevated surface and the resulting thinner troposphere. The significant differences in cloud vertical structures between the TP and the ECP present in this study emphasize that topographical characteristics and the resulting moisture and circulation conditions have strong impacts on the cloud vertical structures.

1. Introduction

Clouds are very important to Earth's climate system. One of the most direct effects imposed by clouds is the modification of the radiative fluxes both at the top of the atmosphere and at the earth's surface. This radiative effect is largely related to the cloud vertical structure (CVS) [1–3]. Because the CVS affects atmospheric circulation by determining the vertical gradient of radiative heating or cooling [4–6], it is very fundamental to accurately describe the geometrical properties like the cloud top height and the cloud layer thickness, as well as the microphysical properties like cloud phase and particle size under various cloud conditions. The effects of CVS on atmospheric radiation and circulation have been studied by a great number of numerical simulations [7]. The parameterization of CVS in the models proved to be critical for the performance of numerical simulations. Since the CVS is highly variable with geographic locations [8, 9], knowledge of the characteristics of CVS is very necessary on distinct topographies such as the Tibetan Plateau (TP hereafter) and the adjacent Eastern China Plains (ECP hereafter).

However, studies are very rare to examine CVS differences between the TP and the ECP for a long time because it is difficult to make routine observations in the plateau, which leads to the lack of available data. Before the application of measurements of remote sensors onboard satellites, a few studies have focused on the clouds over the TP mainly based on the observations of the two Qinghai-Xizang Plateau Meteorology Experiments carried out in 1979 and 1998, respectively [10, 11]. Fortunately, a lot of remote sensing data have been accumulated continually in recent years. The measurements of clouds provided by the International Satellite Cloud Climatology Project (ISCCP) and Moderate Resolution Imaging Spectroradiometer (MODIS) almost

cover the whole globe [12]. These newly available measurements have assembled a few features of the CVS over the TP [13]. For instance, low-level clouds often cover the southern slope of the TP [14]. A lot of deep stratus clouds (primarily the nimbostratus and altostratus) locating on the lee side of the TP during winter and spring are generated and maintained by the frictional and blocking effects [15]. On the contrary, a lot of medium stratiform clouds locating at the eastern TP in cold seasons result from the dynamic effect of the plateau [16]. Although the strongest convection occurs over the Asian monsoon region to the south of the TP, the convective clouds over the TP are shallower and less frequent, and embedded in small-size convective systems [17], and the DCSs over the TP were both weaker and smaller than those over its south slope [18]. Moreover, Precipitation Radar (PR) observations from the Tropical Rainfall Measuring Mission (TRMM) satellite have been analyzed to compare the precipitation type and structure characteristics over the TP and East Asia, implying a large amount of clouds over the TP are weak convective ones [19]. In addition, Yan et al. indicated that the topography-induced compression effect is also shown in the range in the variation of cloud thickness and cloud top height corresponding to different precipitation intensity, which is much smaller over the TP than its neighboring regions [20]. Zhao et al. have indicated that the convection over the Naqu region in the TP could impact rainstorms in the middle and lower reaches of the Yangtze River Basin via a three-dimensional water vapor flux vortex structure [21]. These studies have advanced the knowledge of the differences in CVS over the TP and its surrounding regions.

Nevertheless, Li et al. have pointed out that there is a large underestimation of low-level clouds and overestimation of middle-level clouds over the TP in both ISCCP D2 and the MODIS/Terra cloud products [22]. In addition, the measurements of the PR onboard TRMM satellite, determined mainly by large precipitation-sized hydrometeors, cannot be directly used to depict the vertical structures of clouds. This dilemma has been changed since the CloudSat and CALIPSO satellites were launched and began collecting data routinely [23]. The CPR on CloudSat operates at 94 GHz and directly probes optically thick cloud layers along the satellite orbit [8]. The Cloud-Aerosol Lidar with Orthogonal Polarization (Lidar) on CALIPSO has the unique ability to sense optically thin cloud layers. By combining the two complementary measurements from the two sensors, the merged products are generated by CloudSat Project, which is expected to produce a complete picture of the occurrences of clouds and aerosols in the atmosphere [24, 25]. Sun et al. has used the CloudSat data to analyze the CVS associated with northward advance of the East Asian summer monsoon [26]. Luo et al. has used the joint CloudSat/CALIPSO data to compare deep convective clouds over the TP and Asian monsoon regions, confirming significant differences in the deep convective cloud structures between the two regions [17]. Chen et al. have found that convective clouds over the TP are thinner than those over east China, and the lifetimes of the deep cloud systems over the TP are shorter than those over east China [27]. In this study, we focused on the TP and the ECP to investigate their characteristic CVS. Rather than the deep convective clouds, which constituted only a tiny part of the total amount of clouds (about 1%), all cloud types over both the TP and the ECP in rainy season (from May to August) are analyzed.

2. Data and Methods

In this study, cloud information available in the joint CloudSat/CALIPSO product 2B-GEOPROF-LIDAR [24, 28] was used. The 2B-GEOPROF-LIDAR combined CloudSat CPR and CALIPSO Lidar cloud mask data, containing the cloud top heights and cloud base heights (above sea level) of up to 5 layers at the CloudSat horizontal resolution of ~1.1 km (across and along track). The satellites orbit the earth roughly 14.5 times per day and provide more than 460 000 profiles. During hundreds of days in rainy seasons in year 2006–2009, the total profiles collected all over the globe is more than 200 million. For each $1^\circ \times 1^\circ$ grid in middle latitudes, the average number of profiles is more than 3000.

The data of cloud top height (CTH) were principally used in this study. The CTH was defined as the distance from sea level to the cloud top. Its value was from 0 to 25 km. The occurrences of CTH were the probability of cloud tops were detected at a certain range of height (every 500 m here) in a period of time [29, 30]. Furthermore, the occurrences of CTH for each rainy season in years 2006–2009 were selected and then averaged for the designated areas (e.g., the TP and the ECP) or for each $1^\circ \times 1^\circ$ grid box to get a higher horizontal resolution.

Regions defined in this study are highlighted with polylines in Figure 1. The TP is the area closed by polylines within 28°–39°N and 70°–101°E; the ECP is the area closed by polylines within 29°–37°N and 113°–120°E.

In addition, another CloudSat product called 2B-GEOPROF was used in this study. The 2B-GEOPROF was derived directly from the radar echo of the CPR [8]. It presented a complete picture of cloud body and gave a direct view of the different detection results of clouds between the CPR and the Lidar (e.g., Figures 2(b) and 2(d)). The monthly means from ECMWF Interim Reanalysis project [31] were also used to illustrate the moisture condition, vertical velocity, tropopause height, and temperature profiles over the TP and the ECP in rainy seasons.

3. Comparing CVS with TP and ECP

3.1. Cloud Top. To catch a glimpse of the characteristics of the CVS over the TP and the ECP, we took two tracks numbered 01630 and 01578 as examples to present the profiles of radar reflectivity factor and the cloud layers along the tracks (Figure 2). The track numbered 01630 passed the TP at UTC 07:35 on 18 Aug, 2006. The surface altitude almost is 5 km above the footprints in the TP along the track. A few isolating and small convective clouds were detected by the CPR. They extended from the surface to the high altitude, with the top height of about 13 km and the thickness of about 7 km. There were still some cloud layers revealed by the information of Lidar above the cloud top detected by the

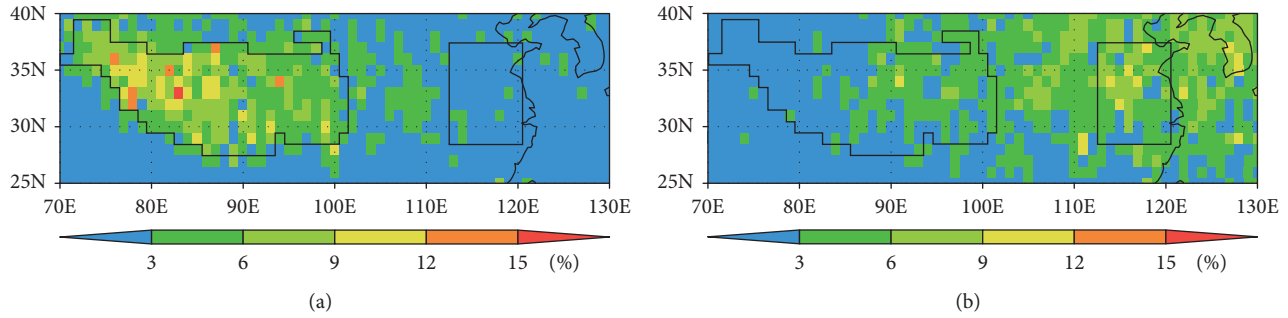

Figure 1: Occurrence averaged vertically for (a) range A and (b) range B both ranges A and B are defined as in Figure 3. The left closed region represents the TP, and the right closed region represents the ECP.

CPR. These cloud layers were over 15 km in height but less than 2 km in thickness. Detected by the Lidar but not the CPR, they were likely to be tenuous. The track numbered 01578 passed the ECP at UTC 18:23 on 14 Aug, 2006. The surface is flat and has an averaged altitude below 200 m along the track. There was a deep convective cloud detected by the CPR. It extended vertically from near the surface to about 17 km, with a thickness of more than 15 km and a horizontal scale of about hundreds of kilometers. Surrounding the top of the deep convective cloud, there was a large cloud anvil detected by the Lidar. It is clear that there are different characteristics in size and thickness of the convective clouds over the TP and the ECP in rainy season. In addition, Figure 2 also revealed two pieces of important information. Firstly, a lot of tenuous clouds and anvils were omitted by the CPR but detected by the Lidar, indicating the 2B-GEOPROF-LIDAR data combined from both the CPR and the Lidar have the potential of providing a more complete picture of the occurrences of clouds than the data from the CPR only. Secondly, some high-level clouds and anvils overlapped over the low-level clouds formed multilayered clouds. Since more clouds were obtained from 2B-GEOPROF-LIDAR, it was used rather than 2B-GEOPROF to analyze the detail CVS over the TP and the ECP in this study.

Cloud top height is the most intuitive parameter reflecting the CVS. The vertical variation of the occurrences of CTH is presented in Figure 3. The maximum of the occurrences (about 6.5%) over the TP is at the height of 7.5 km. This height is slightly larger than the average top height of low-level clouds reported in[25]. The reason is that we defined only the core plateau as the TP (Figure 1), where the average altitude of the surface is much higher. By added with the higher elevation of surface, the average height of cloud tops is higher too. The occurrences over the ECP are large near the surface (about 3% at 1 km), but the globe maximum (about 5%) is found at the height of 11.5 km, which is 4 km higher than that of the TP.

To realize the horizontal distribution of the clouds over the TP and the ECP, we averaged the occurrences of CTH vertically for the range A and range B over the TP and the ECP, respectively, where the most concentrated cloud tops were found (Figure 3). The distribution of averaged occurrences of range A shows a good correspondence with topography (Figure 1(a)). The occurrences are biggest in the western part of the TP and decreases gradually from west to east. It is clear that the great bigger occurrences over the TP than its surrounding regions, indicating that the topography conditions are the leading factor in affecting the CTH over the TP. However, the distribution of averaged occurrences of range B is not significantly related to the topographies. It increases gradually from west to east and peaks in the ECP and the offshore regions. The different characteristics in horizontal distribution of clouds suggest that it is other one rather than topographies dominating the CTH over the ECP.

Since the CTH is much different over the TP and the ECP, the cross sections of the occurrences along longitude and latitude were examined to get more detailed vertical variation of it, as shown in Figure 4. The maximum occurrence in the vertical direction is located at the height of 7-8 km. Although the upper boundary of CTH over the TP is about 18 km, the occurrences of the CTH ranging from 10 to 18 km are very tiny. From the TP to the ECP, the upper boundary of CTH descends slightly, but the height of the maximum occurrence (HMO) increases greatly. The increasing of the HMO is sharpest over the Sichuan Basin located just on the east of the TP. It gets to the peak value exceeding 12 km over the ECP. On the contrary, the occurrences of the CTH ranging from 3 to 10 km are very small over the ECP. It is clearly found that the cloud top is elevated from the TP to the ECP, although the surface elevation continues to fall.

The variation of CTH over the TP is also notable along latitude. Most cloud top is above 15 km in the south of the TP, which has intense convection in boreal summer. Although the TP is adjacent to it, the most CTH over the TP is only 6–8 km. Low CTH is the most important characteristic of the TP's clouds differing with that of its surrounding regions and the ECP. Without big mountains disturbing the boundary layer, the variation of CTH over the ECP is rather monotonous. The HMO over the ECP descends gradually with the increased latitude and always keeps over 10 km.

The comparison of CTH over the TP and ECP shows that the clouds is much lower (from sea level) over the TP than its surrounding regions and the ECP, although they maintain on the highly elevated surface. This is consistent with previous reports of the weaker deep convection and shallower deep clouds over the TP [17, 18].

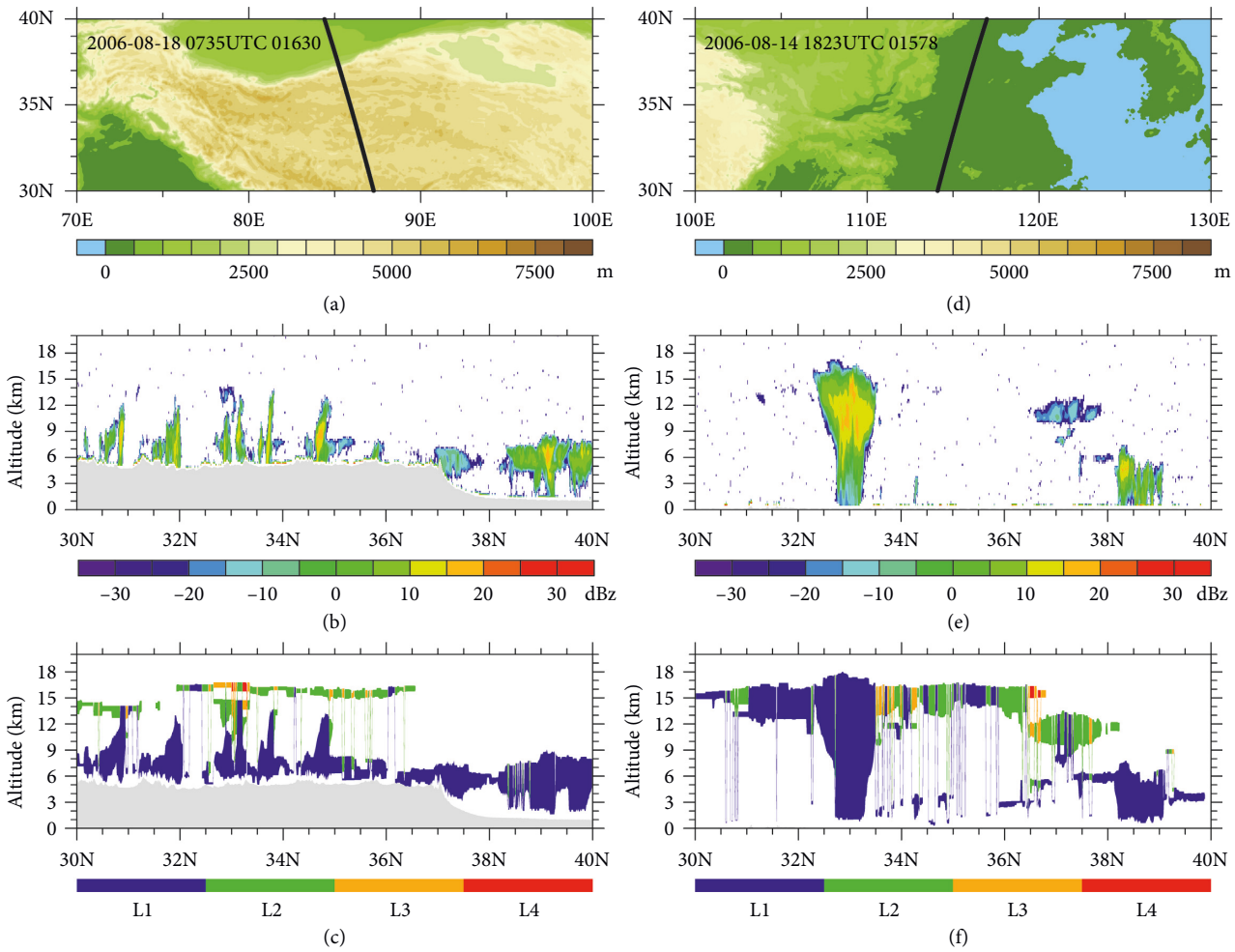

FIGURE 2: Two cases of clouds over the TP (left panel) and ECP (right panel) detected by CPR and Lidar. (a) and (d): location of the tracks (black solid line) over different elevation area (color shading); (b) and (e): radar reflectivity measured in dBZ (color shading) along the tracks; and (c) and (f): vertical stratification of the clouds, L1 to L4 represent the separate cloud layers from bottom to top.

3.2. Cloud Classification. As emphasized by Li et al. [22], the cloud classification should be modified over the TP. Elevated by the surface mountains, the low-level clouds and middle-level clouds over the TP are difficult to be distinguished as usual. A feasible scheme for classifying clouds over the TP and the ECP is thus necessary. Wood [32] had pointed out that the portion of the cloud profile colder than −20°C is deemed pure ice, and the portion of the profile warmer than 0°C is considered pure liquid. We also considered the cloud top temperature to be crucial in classifying clouds, and thereby the climatologically averaged temperature profiles over the TP and the ECP were examined primarily (Figure 5). The temperature is slightly lower over the TP than that over the ECP at the height of below 10 km. The difference between them is about 2°C at the height of 5 km and then decreases with height. We treated the freezing level (the height of 0°C) as the borderline separating warm clouds from mixed-phase clouds, and the crystal level (the height of −20°C) as the borderline between the mixed-phase clouds and ice clouds. Therefore, the warm clouds, mixed-phase clouds, and ice clouds over the TP are defined, respectively, as that whose top heights are below 6.0 km, between 6.0 and 9.2 km, and above 9.2 km, respectively. Accordingly, the cloud top heights of the three cloud types over the ECP are below 5.5 km, between 5.5 and 9.0 km, and above 9.0 km, respectively.

Figure 6 shows the horizontal distribution of occurrences for warm clouds, mixed-phase clouds, and ice clouds. The warm clouds are infrequent over the TP. Meanwhile, the warm clouds have the largest occurrences just east to the TP and show prevalence in the downstream of the TP. It clear that the characteristics of downstream flows of plateau are favorable for the development of warm clouds, which often develop in stably stratified and weak turbulence low-level atmosphere [17, 21]. The largest occurrences of mixed-phase clouds are found to locate just over the TP, where it is more than 30%. On the contrary, the mixed-phase clouds are infrequent over the ECP. The occurrences of them are less than 10% in a big area of the ECP. Compared to the warm clouds and mixed-phase clouds, the ice clouds have the most insignificant difference between the TP and the ECP. The occurrences of ice clouds decrease gradually with increased latitude over the both regions. It seems to be more closely

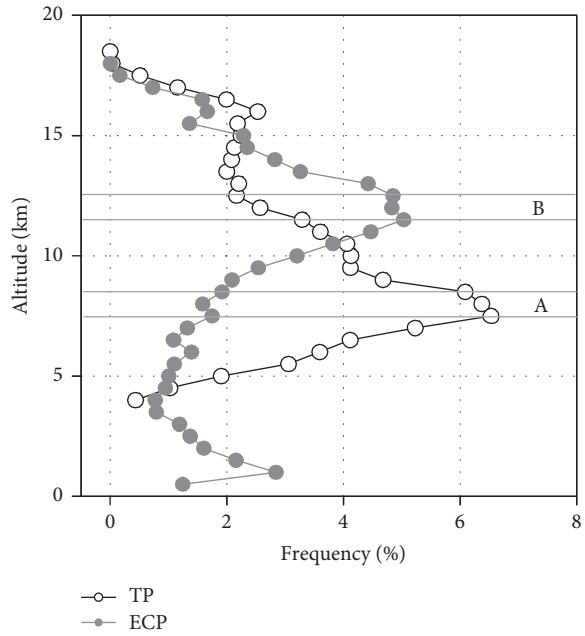

Figure 3: The regionally averaged occurrence of CTH over the TP and the ECP.

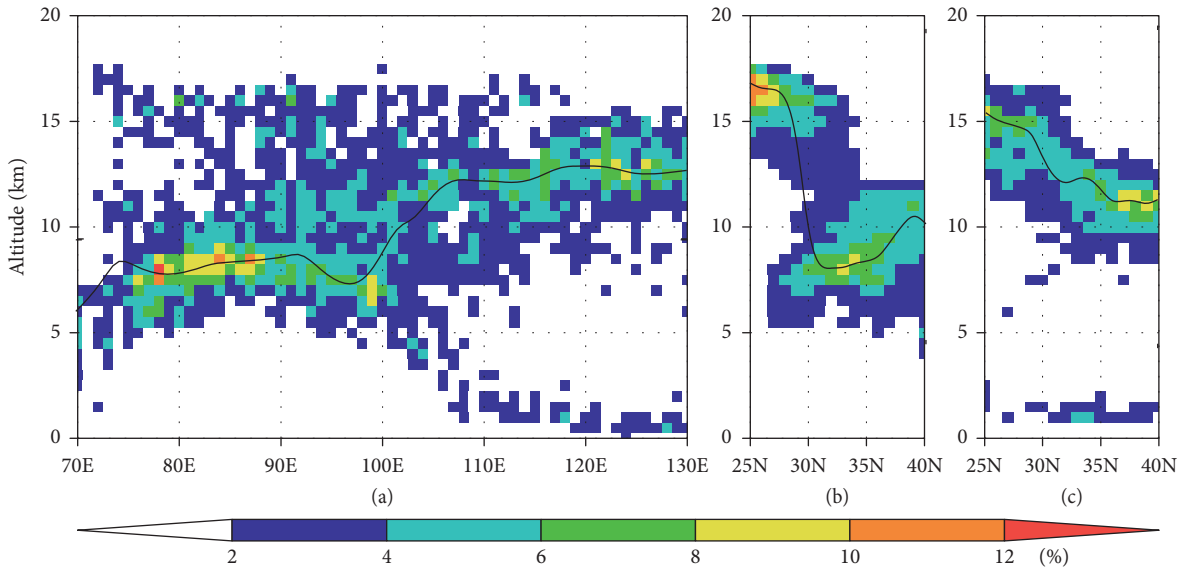

Figure 4: Cross sections of occurrence of CTH along longitude (a) averaged between 30°N and 35°N and latitude (b) averaged between 80°E and 95°E and (c) averaged between 110°E and 120°E. The thick solid line represents the height of maximum values.

related to its location of latitude rather than the topographies of lower boundary.

We also examined the thicknesses of the warm clouds, mixed-phase clouds, and ice clouds. Figure 7 shows the probability density (PD) of the thicknesses of the three cloud types individually. The warm clouds are generally thin, with thickness hardly more than 3 km over the TP. However, the thickness of some warm clouds over the ECP is large (up to 6 km), although their PD is small. Most mixed-phase clouds over the TP are less than 3 km, while a large number of mixed-phase clouds over the ECP are thicker than 5 km. The thickness of ice clouds is significantly different between the two regions. The PD of cloud thickness around 4–8 km is about 2% higher over the TP than that over ECP. However, there is almost no ice cloud thicker than 10 km over the TP, while it is about 1% over the ECP.

The comparison of cloud classification and its thickness reveals that there are two representative forms of cloud over the TP, the one is mixed-phase cloud and the other is medium-thickness ice cloud. On the contrary, there are two representative forms of the cloud over the ECP too, the one is low-level warm cloud, and the other is large-thickness ice cloud. The reasons for the difference in the CVS between the TP and the ECP are discussed in Section 4.

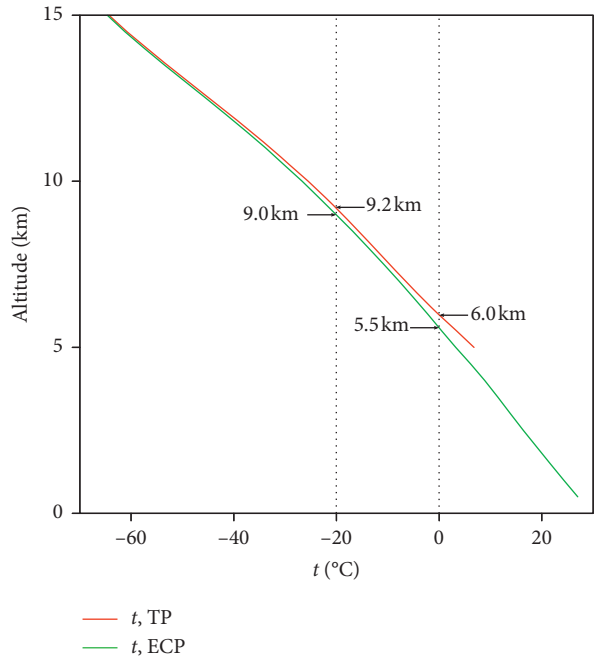

Figure 5: Vertical profiles of temperature.

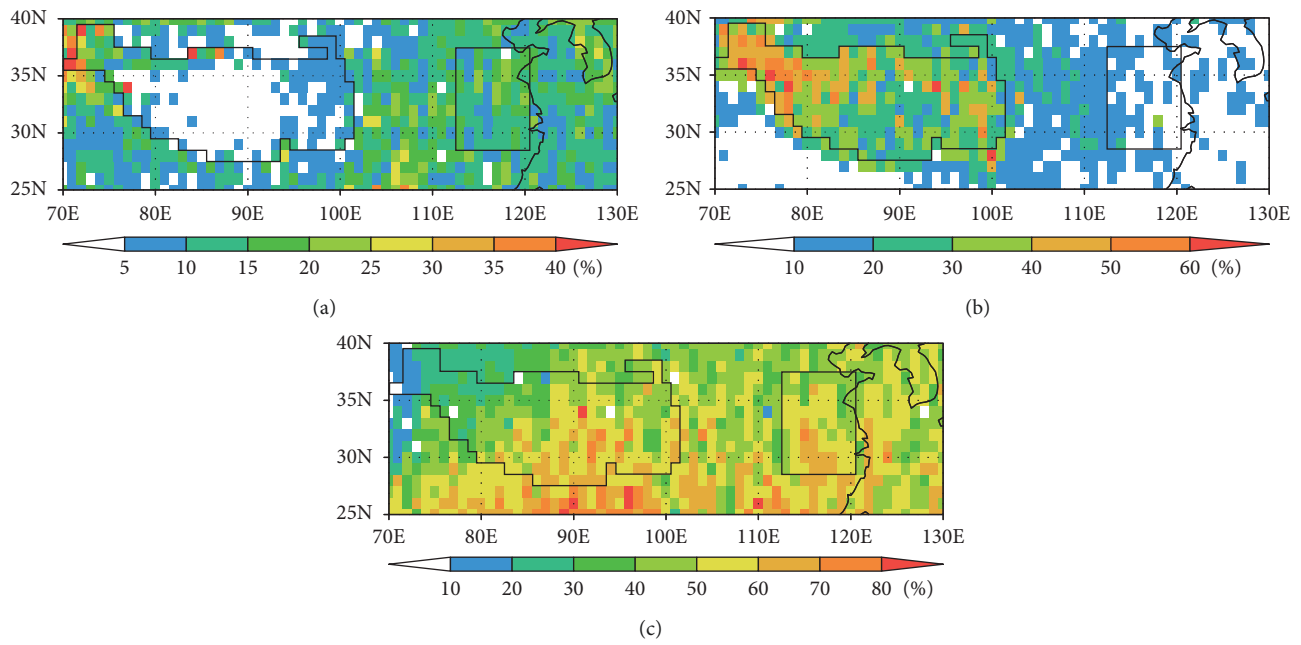

Figure 6: Occurrence distributions of (a) warm clouds, (b) mixed-phase clouds, and (c) ice clouds.

3.3. Multilayered Clouds. In addition to top height and classification, vertical stratification of the clouds is also an important property of the CVS. The measurements of clouds as combined observed by the CPR and the Lidar have an outstanding ability to identify more than one cloud layer overlapped. It is easy to collect the information of the number of cloud layers, top height, and base height of each cloud layer for a given profile by using the 2B-GEOPROF-LIDAR data. The statistic results of the occurrences of single-layered clouds and multilayered clouds during rainy seasons are presented in Table 1. Single-layered clouds are the prominent type over both the TP (62%) and the ECP (51%), two-layered clouds ranks second with a similar percentages over the TP (21%) and over the ECP (20%), and three-layered clouds are much less (only 3% over the TP and 4% over the ECP). Since the clouds with four to five layers are rare (less than 1%), they are not discussed in this study.

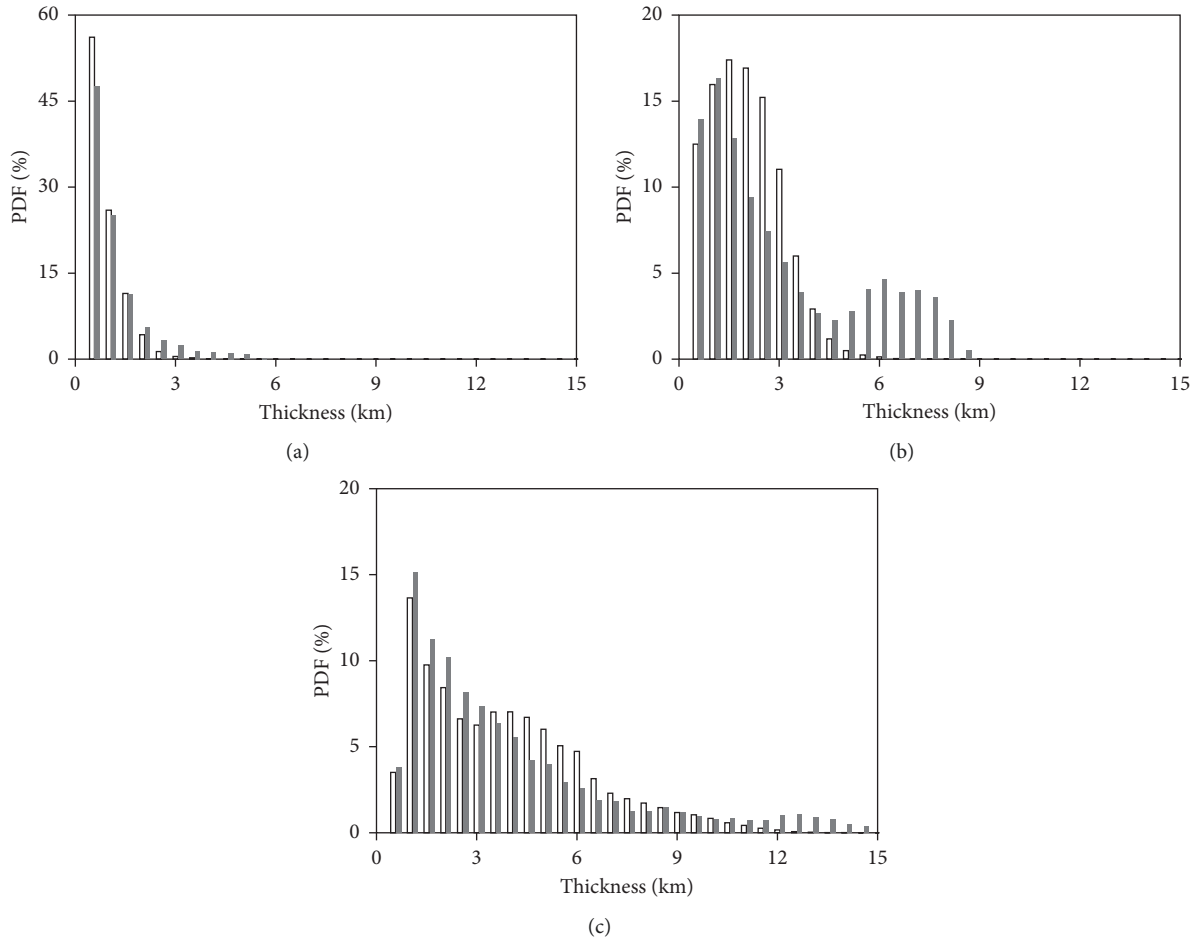

Figure 7: Probability density of thickness for (a) warm clouds, (b) mixed-phase clouds, and (c) ice clouds.

Table 1: Occurrence of multilayered clouds (%).

Region	Clear sky	Single-layered	Two-layered	Three-layered
TP	12.92	62.29	20.74	3.03
ECP	23.63	50.65	20.25	4.26

Figure 8 shows the occurrences of single-layered clouds, two-layered clouds, and three-layered clouds. The distribution of single-layered clouds shows a good agreement with the topographies of high land. Larger occurrences of single-layered clouds are a significant characteristic of the TP, especially over the western parts. The steady mechanical lifting on the windward slope sustained by low-level westerly flows is favorable for the forming of continuous shallow clouds. Weak convections prevailing in the summer TP may also play a role in it. The distribution of multilayered clouds, both the two-layered clouds and three-layered clouds, does not show a significant consistency with the topographies. The occurrences of multilayered clouds is depressive towards high latitude. We found the largest occurrences of multilayered clouds to south of the TP, where the deep convections are most frequent. As presented in Figure 2, deep convective clouds generally cover a vast area and have a bulky vertical extent as huge umbrellas, increasing the probability of cloud layers to be overlapped. High cirrus from residual deep convective clouds also has contribution to the occurrences of multilayered clouds.

Figure 9 shows the mean top height of the cloud layer of single-layered and multilayered clouds and its variance. The single-layered clouds over the TP and the ECP are almost the same in mean top height. But the mean top height of cloud layers over the TP is higher than that over the ECP. Especially, this bias in top height is largest in the lowest cloud layers and becomes smaller and smaller in the upper cloud layers. On the contrary, the cloud layers over the TP are thinner than that over the ECP, including both the single-layered clouds and the multilayered clouds (Table 2).

4. Discussion

As mentioned in Section 3, mixed-phase clouds and medium-thickness ice clouds are most representative over the TP, while warm clouds and large-thickness ice clouds are most representative over the ECP. We put forward that the differences in the CVS are mainly attributed to the distinct topographies and resulting moisture condition and atmospheric circulation. During most of the year, the TP has the highest rate of warming in the northern hemisphere. The low-level warming sustains strong lifting to initiate the

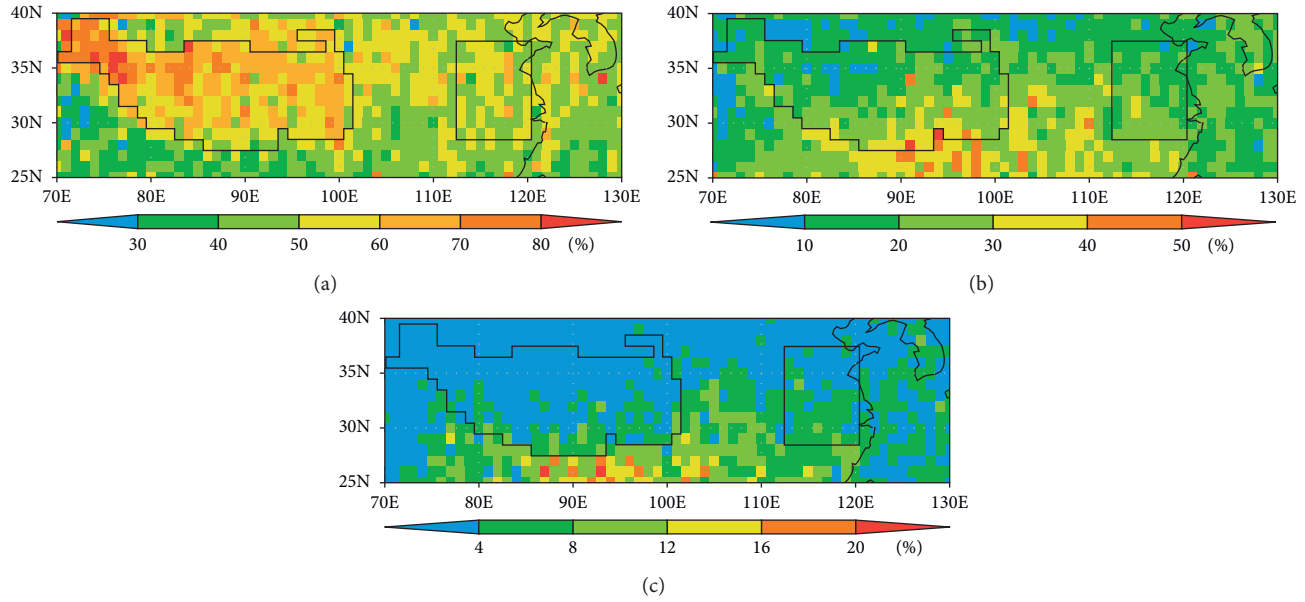

Figure 8: Occurrence distributions of (a) single-layered clouds, (b) two-layered clouds, and (c) three-layered clouds.

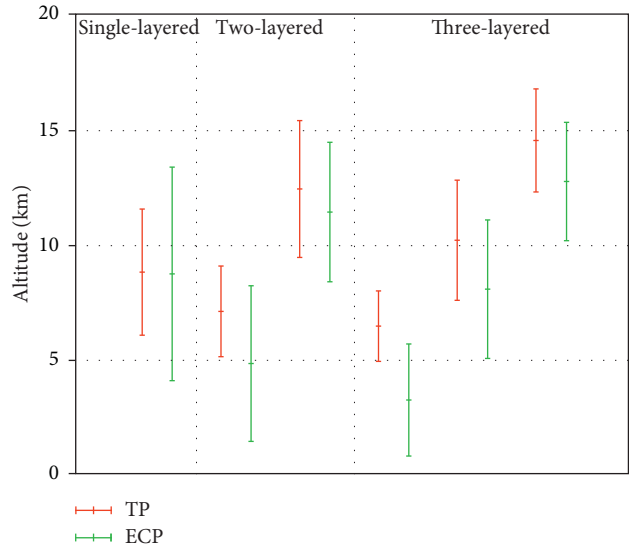

Figure 9: Mean top height of the cloud layers of (a) single-layered, (b) two-layered, and (c) three-layered clouds. The error bars represent standard errors of the means.

Table 2: Average thickness of cloud layers of single-layered and multilayered clouds (km).

Region	Single-layered	Two-layered		Three-layered		
		FL	SL	FL	SL	TL
TP	3.24 ± 2.35	2.02 ± 1.62	2.13 ± 1.49	1.56 ± 1.22	1.56 ± 1.11	1.79 ± 1.18
ECP	3.84 ± 3.55	2.20 ± 2.32	2.37 ± 1.76	1.59 ± 1.76	1.59 ± 1.19	1.87 ± 1.27

Statistical results are expressed as mean ± variance. The FL, SL, and TL mean the first, second, and third cloud layer from surface to upper.

convective motion. As shown in Figure 10, the TP has the largest vertical velocity in the Eastern Asia between 30°N and 35°N. In addition, because the low-level air approaches saturation nearest, it is favorable for the development of convections and clouds formed within them. However, from the increased depression of the dew point with height, it is clearly found that the air becomes more and more unsaturated in high levels. A dry environment is unfavorable for deep convection because the entrainment of drier environmental air leads to stronger evaporative cooling and

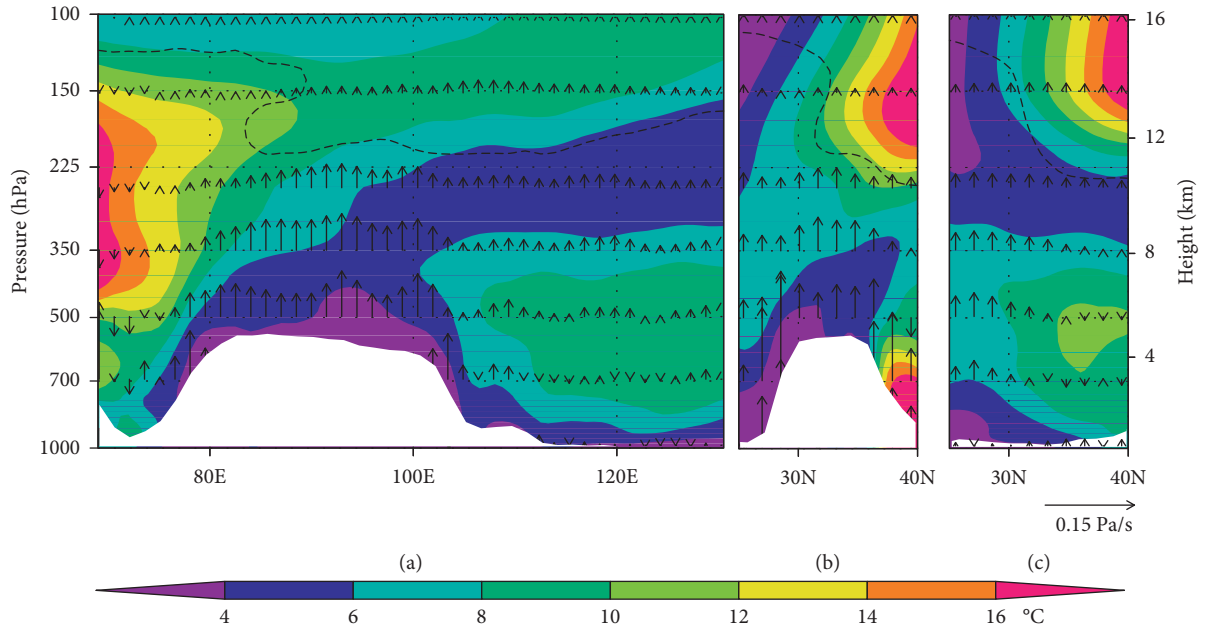

Figure 10: Cross sections of depression of the dew point and vertical velocity along longitude (a) averaged between 30°N and 35°N and latitude (b) averaged between 80°E and 95°E and (c) averaged between 110°E and 120°E. A scale of vertical velocity is shown on the lower-right of the figure, and its units is Pa/s. The thick dashed line represents dynamic tropopause.

negative buoyancy so that the convections over the TP are difficult in transit from shallow to deep. On the contrary, the convection over the TP is usually small in size (Figure 2). Because small-size clouds are more likely to be diluted by mixing with dry air, they are not expected to have bulky vertical extent.

Located downstream of the TP, the circulation of the ECP is significantly influenced by the blocking and frictional effects of big mountains. The downstream low-level convergence sustains large-scale steady lifting, while the mid-tropospheric westerly flows slowed down by the mountainous surface generate downstream midlevel divergence, resulting in the lifting is confined to the low troposphere. Figure 10 shows that the downstream flows are climatologically weak uplifting or sinking and are most unsaturated in midlevels. This environment is unfavorable for the generation and development of clouds in midlevels, resulting in the smaller occurrences of mixed-phase clouds over the ECP. But why large-thickness ice clouds have a higher occurrence over the ECP than those over the TP? This could be explained in terms of the impacts of Asian monsoon. Deep convective clouds are the main source of large-thickness ice clouds. Kuang and Bretherton [33] had put forth that the development of deep convection depends on the moisture content of the free troposphere. Under the control of Asian summer monsoon, abundant water vapor is converged over the ECP by the transportation of monsoon flows, making shallow convections rapidly develop into deep ones after moisture is added [34]. Strong synoptic-scale systems occurs frequently over the ECP in summertime, and the deep convections associated with them are much larger in size than that over the TP. Large-size clouds shield them from deleterious effects of environment to maintain the buoyancy of saturated updrafts. In addition, the increased saturation level with height of environment air is more favorable compared with that of the TP for maintaining and enhancing the deep convection too (Figure 10).

5. Conclusion

The CVS that is important in the atmospheric radiation was examined over two designated regions, the TP and the ECP, by using the 2B-GEOPROF-LIDAR data. Based on the case analysis and statistic calculation of the clouds during rainy season in 2006–2009, the characteristics of cloud top height, cloud type, cloud thickness, and the number of vertical cloud layers were revealed. Many distinct cloud features between the TP and the ECP were clarified.

Without the influence of topographies on clouds, the analysis of clouds over the ECP was documented and regarded as a reference. Over the ECP, the maximum occurrence of CTH is found to be 5.1% occurring at 11.5 km. This height is above the crystal level so that the ice clouds are the predominant cloud type. A lot of ice clouds have thickness more than 10 km. Mixed-phase clouds are another type that has lower cloud top height between the crystal level and the freezing level. They are infrequent over the ECP. Warm clouds have no occurrences as large as the ice clouds. They are lower top and shallow extent, prevailing downstream of the TP. From the statistical results of multiply layers of clouds, it is found that single-layered clouds are dominant with an averaged occurrence of more than 50%, although a rather remarkable percentage of clouds have more than one vertical cloud layer. The percentage of multilayered clouds decreases sharply with the increased number of their vertical cloud layers.

As is well known, the main body of the TP is the highest region on the earth. The most notable difference of CVS with that over the ECP is the height of maximum occurrence of CTH. It is found to be 6.6% at 7.5 km, which is 4 km lower than that of the ECP. The height of maximum occurrence is below the crystal level but above the ice level. Therefore, mixed-phase clouds rather than ice clouds become the predominant type. Mixed-phase clouds over the TP are usually thinner than 5 km. The PD of cloud thickness manifests the prominent distinctions of ice clouds between the TP and the ECP. The PD of cloud thickness is about 2% higher over the TP around 4–8 km but extremely lower exceeding 10 km, while it is about 1% over the ECP. Moreover, the cloud layers of multilayered clouds are higher and thinner over the TP than over the ECP.

These distinct features in the CVS over the TP and the ECP are closely related to the atmospheric environment affected by topographies. Initiated by low-level warming, convective activities are frequent over the TP. But the convections are difficult to transit from shallow to deep due to the rapidly diminished moisture with height. Shallow convections prevailing over the TP increase the PD of mixed-phase clouds and ice clouds with medium thickness. Located downstream of the TP, the lifting over the ECP is climatologically confined to the lower troposphere, leading to the less of mixed-phase clouds. On the contrary, the ECP is under the control of Asian monsoon, which has routinely intense synoptic-scale cyclone activities in summer. Deep convections and strong precipitations usually occur associated with the development of synoptic-scale systems, resulting in the increased probability of ice clouds that consist of deep convective clouds and high cirrus from their residual.

Based on the analysis of properties of the CVS, an extended knowledge of the clouds over the plateau and the plains was presented. These detailed characteristics of the CVS present a close linkage of it and the circulation environment on different topographies. These results are critical in understanding the impacts of topographies on the climate and may be necessary for the parameterization of clouds in numerical models.

Data Availability

The CloudSat/CALIPSO data used to support the findings of this study may be released upon application to the CloudSat Data Processing Center (CloudSat DPC), who can be contacted at cloudsat@colostate.edu.

Conflicts of Interest

The author declares that there are no conflicts of interest regarding the publication of this paper.

Acknowledgments

The author greatly appreciates the NASA CloudSat project for providing the CloudSat/CALIPSO dataset and the ECMWF Interim Reanalysis project for providing the monthly data. This work was funded by the National Basic Research Program of China (41105031 and 91337213), Key Research and Development Plan of Anhui Province (1804a0802196), and National Key Research and Development Plan (2018YFC0213806).

References

[1] F. Richter, K. Barfus, F. H. Berger, and U. Görsdorf, "The influence of cloud top variability from radar measurements on 3-D radiative transfer," *Atmospheric Chemistry and Physics*, vol. 7, no. 17, pp. 4699–4708, 2007.

[2] T. Várnai and R. Davies, "Effects of cloud heterogeneities on shortwave radiation: comparison of cloud-top variability and internal heterogeneity," *Journal of the Atmospheric Sciences*, vol. 56, no. 24, pp. 4206–4224, 1999.

[3] P. J. Webster and G. L. Stephens, "Tropical upper-tropospheric extended clouds: inferences from winter MONEX," *Journal of the Atmospheric Sciences*, vol. 37, no. 7, pp. 1521–1541, 1980.

[4] Z. Feng, X. Dong, B. Xi, C. Schumacher, P. Minnis, and M. Khaiyer, "Top-of-atmosphere radiation budget of convective core/stratiform rain and anvil clouds from deep convective systems," *Journal of Geophysical Research: Atmospheres*, vol. 116, no. 23, 2011.

[5] W. Li, C. Schumacher, and S. A. McFarlane, "Radiative heating of the ISCCP upper level cloud regimes and its impact on the large-scale tropical circulation," *Journal of Geophysical Research: Atmospheres*, vol. 118, no. 2, pp. 592–604, 2013.

[6] T. Vaillant de Guélis, H. Chepfer, V. Noel et al., "The link between outgoing longwave radiation and the altitude at which a spaceborne lidar beam is fully attenuated," *Atmospheric Measurement Techniques*, vol. 10, no. 12, pp. 4659–4685, December 2017.

[7] J. Wang and W. B. Rossow, "Effects of cloud vertical structure on atmospheric circulation in the GISS GCM," *Journal of Climate*, vol. 11, no. 11, pp. 3010–3029, 1998.

[8] G. G. Mace, R. Marchand, Q. Zhang, and G. Stephens, "Global hydrometeor occurrence as observed by CloudSat: initial observations from summer 2006: CLOUDSAT hydrometeor occurrence," *Geophysical Research Letters*, vol. 34, no. 9, 2007.

[9] E. Weisz, J. Li, W. P. Menzel, A. K. Heidinger, B. H. Kahn, and C.-Y. Liu, "Comparison of AIRS, MODIS, CloudSat and CALIPSO cloud top height retrievals," *Geophysical Research Letters*, vol. 34, no. 17, 2007.

[10] J. Yang, S. Tao, Z. Gu, and D. Ye, *Meteorology of Tibetan Plateau*, Science Press, Beijing, China, 1960.

[11] D. Ye and Y. Gao, *Meteorology of the Qinghai-Xizang Plateau*, Science Press, Beijing, China, 1979.

[12] W. B. Rossow and R. A. Schiffer, "Advances in understanding clouds from ISCCP," *Bulletin of the American Meteorological Society*, vol. 80, no. 11, pp. 2261–2287, 1999.

[13] B.-C. Gao, P. Yang, G. Guo, S. K. Park, W. J. Wiscombe, and B. Chen, "Measurements of water vapor and high clouds over the Tibetan plateau with the terra modis instrument," *IEEE Transactions on Geoscience and Remote Sensing*, vol. 41, no. 4, pp. 895–900, 2003.

[14] Y. Kurosaki and F. Kimura, "Relationship between topography and daytime cloud activity around Tibetan plateau," *Journal of the Meteorological Society of Japan*, vol. 80, no. 6, pp. 1339–1355, 2002.

[15] R. Yu, B. Wang, and T. Zhou, "Climate effects of the deep continental stratus clouds generated by the Tibetan plateau," *Journal of Climate*, vol. 17, no. 13, pp. 2702–2713, 2004.

[16] Y. Li, R. Yu, and Y. Xu, "The formation and diurnal changes OF stratiform clouds IN southern China," *Acta Meteorologica Sinica*, vol. 61, no. 6, pp. 733–743, 2003.

[17] Y. Luo, R. Zhang, W. Qian, Z. Luo, and X. Hu, "Intercomparison of deep convection over the Tibetan plateau-Asian monsoon region and subtropical north America in boreal summer UsingCloudSat/CALIPSO data," *Journal of Climate*, vol. 24, no. 8, pp. 2164–2177, 2011.

[18] G. Gao, Q. Chen, H. Cai, Y. Li, and Z. Wang, "Comprehensive characteristics of summer deep convection over Tibetan plateau and its south slope from the global precipitation measurement core observatory," *Atmosphere*, vol. 10, no. 1, 9 pages, 2019.

[19] Y. Fu, G. Liu, G. Wu et al., "Tower mast of precipitation over the central Tibetan Plateau summer," *Geophysical Research Letters*, vol. 33, no. 5, 2006.

[20] Y. Yan, Y. Liu, and J. Lu, "Cloud vertical structure, precipitation, and cloud radiative effects over Tibetan Plateau and its neighboring regions," *Journal of Geophysical Research: Atmospheres*, vol. 121, no. 10, pp. 5864–5877, 2016.

[21] Y. Zhao, X. Xu, L. Liu et al., "Effects of convection over the Tibetan plateau on rainstorms downstream of the Yangtze River basin," *Atmospheric Research*, vol. 219, pp. 24–35, 2019.

[22] Y. Li, X. Liu, and B. Chen, "Cloud type climatology over the Tibetan Plateau: a comparison of ISCCP and MODIS/TERRA measurements with surface observations," *Geophysical Research Letters*, vol. 33, no. 17, 2006.

[23] G. L. Stephens, D. G. Vane, R. J. Boain et al., "The cloudsat mission and the A-train," *Bulletin of the American Meteorological Society*, vol. 83, no. 12, pp. 1771–1790, 2002.

[24] G. G. Mace et al., "A description of hydrometeor layer occurrence statistics derived from the first year of merged Cloudsat and CALIPSO data," *Journal of Geophysical Research*, vol. 114, 2009.

[25] C. M. Naud and Y.-H. Chen, "Assessment of ISCCP cloudiness over the Tibetan plateau using CloudSat-CALIPSO," *J. Geophys. Res.*, vol. 115, no. 10, 2010.

[26] G. Sun, Y. Li, and J. Lu, "Cloud vertical structures associated with northward advance of the East Asian summer monsoon," *Atmospheric Research*, vol. 215, pp. 317–325, 2019.

[27] J. Chen, X. Wu, Y. Yin, Q. Huang, and H. Xiao, "Characteristics of cloud systems over the Tibetan plateau and east China during boreal summer," *Journal of Climate*, vol. 30, no. 9, pp. 3117–3137, 2017.

[28] G. Stephens, D. Winker, J. Pelon et al., "CloudSat and CALIPSO within the A-train: ten years of actively observing the earth system," *Bulletin of the American Meteorological Society*, vol. 99, no. 3, pp. 569–581, 2018.

[29] S.-W. Kim, E.-S. Chung, S.-C. Yoon, B.-J. Sohn, and N. Sugimoto, "Intercomparisons of cloud-top and cloud-base heights from ground-based Lidar, CloudSat and CALIPSO measurements," *International Journal of Remote Sensing*, vol. 32, no. 4, pp. 1179–1197, 2011.

[30] K. L. Verlinden, D. W. J. Thompson, and G. L. Stephens, "The three-dimensional distribution of clouds over the southern hemisphere high latitudes," *Journal of Climate*, vol. 24, no. 22, pp. 5799–5811, 2011.

[31] D. P. Dee, "The ERA-Interim reanalysis: configuration and performance of the data assimilation system," *Quarterly Journal of the Royal Meteorological Society*, vol. 137, no. 656, pp. 553–597, 2011.

[32] N. Wood, *Level 2B Radar-Visible Optical Depth Cloud Water Content (2B-CWC-RVOD) Process Description Document*, Cooperative Institute for Research in the Atmosphere (CIRA), Fort Collins, CO, USA, 2008.

[33] Z. Kuang and C. S. Bretherton, "A mass-flux scheme view of a high-resolution simulation of a transition from shallow to deep cumulus convection," *Journal of the Atmospheric Sciences*, vol. 63, no. 7, pp. 1895–1909, 2006.

[34] M. Yi, Y. Fu, P. Liu, Y. Gao, and X. Hong, "Analysis of the variation of atmospheric composition in the upper troposphere during a strong convection in eastern China in summer," *Chinese Journal of Atmospheric Sciences*, vol. 36, no. 5, pp. 901–911, 2012.